Optical and Electrical Characterization and Modeling of Photon Detection Probability in CMOS Single-Photon Avalanche Diodes

H. Mahmoudi, S. S. Kohneh Poushi, B. Steindl, M. Hofbauer, and Horst Zimmermann

***Abstract*— Single-photon avalanche diodes (SPADs) are very attractive devices in optical detector applications where both CMOS integration and low light detection are critical. An important SPAD performance parameter is the photon detection probability (PDP) which has to be carefully characterized for the sensor design. In this paper, we present a comprehensive modeling and experimental characterization of the PDP to obtain its optical and electrical dependency on different parameters including the wavelength and light incidence angle as well as the biasing condition.**

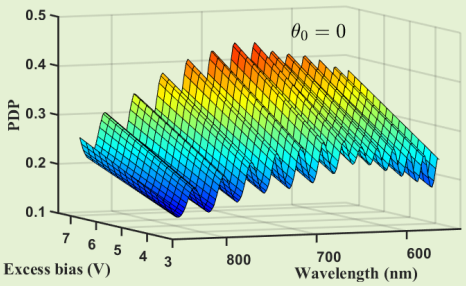

By calculating the optical absorption and the avalanche triggering probabilities within the silicon, the PDP of an n^+/p-well CMOS-implemented SPAD is accurately modeled. It is shown that due to the formation of a standing wave in different layers above the silicon, which significantly affects the optical transmission and the PDP spectrum, the application of the presented approach is necessary especially when an anti-reflection coating layer is not available. The obtained result shows an excellent agreement to our measurements and, therefore, the model can be reliably used for accurate design and optimization of SPAD-based detectors and to avoid very time-consuming experimental investigations, e. g. for obtaining the detector performance for deviations in the light incidence angle.

***Index Terms*— Optical transmission, photon absorption profile, photon detection probability (PDP), single-photon avalanche diode (SPAD).**

I. Introduction

DUE to the high sensitivity down to a single photon and the CMOS realization, single-photon avalanche diodes (SPADs) have become attractive candidates in different optical detection applications such as quantum cryptography, fluorescence microscopy, time-of-flight sensors and optical wireless communication [1]–[6]. The SPAD operation can be thought as a simple diode which is reversely biased above its avalanche breakdown voltage and, therefore, an absorbed photon in the depletion region can generate an electron-hole pair reaching a multiplication region, where a strong electric field accelerates the carriers to gain enough kinetic energy to create a self-sustaining avalanche. The self-sustaining avalanche has to be extinguished by reducing the reverse bias voltage to below the breakdown by a quenching circuit. This circuit can be a simple resistor (passive quenching) to drop the voltage or based on a more complex circuitry where the avalanche is detected and quenched (active quenching) [7], [8]. Then, in order to recover (reset) the SPAD for the next detection, the reverse bias is raised again to a voltage level above the breakdown [9].

The key factor to determine the sensitivity of the SPAD is called photon detection probability (PDP). In order to characterize the PDP, its dependency on different optical and electrical parameters including the wavelength and angular deviation from the surface normal of the incident light as well as the biasing condition has to be taken into account. Recently, a physics-motivated modeling and simulation approach has been presented to characterize the PDP based on the parameterization of the avalanche triggering probability throughout the silicon [10]–[15]. As the avalanche triggering probability strongly depends on the position (depth) of the electron-hole generation inside the silicon, the accurate determination of photon absorption profile is necessary. This is especially important, when an anti-reflection coating layer is not available as it is the case with many CMOS process technologies.

Unfortunately, this effect has been ignored in the above-mentioned model and, as it is shown in this paper, due to the formation of a standing wave in different layers above the silicon, the optical transmission into the silicon and the PDP spectrum of the SPAD show a strong dependency on the wavelength as well as the angular deviation from the surface normal of the incident light. In contrast to [16], where we investigated a high-voltage CMOS process, in this paper, we extend the approach of [11]–[14] and apply it to a standard CMOS process to obtain a comprehensive PDP model

Manuscript received September XX, 2020. This work was supported in part by the Austrian Science Fund (FWF) under grant no. P28335-N30.

The authors are with Institute of Electrodynamics, Microwave and Circuit Engineering, Vienna University of Technology, Vienna 1040, Austria (e-mail: hiwa.mahmoudi@tuwien.ac.at).

Digital Object Identifier XX/XXX.

which carefully combines optical and electrical simulations and captures the complex dependencies of PDP to wavelength, excess bias, and light incident angle. In order to verify our model, spectral and excess bias dependencies of the PDP for a SPAD with n^+/p-well structure (Fig. 1) is calculated and compared with measured results. The presented approach enables precise device characterization and provides insight into geometrical, wavelength and voltage bias dependencies of the PDP as a key design parameter to achieve further improvements in SPAD-based applications.

The reminder of the paper is organized as follows. Sec. II describes the SPAD structure and our measurement setup. In Sec. III we explain the basis of the PDP modeling and afterwards we present our approach to achieve a comprehensive model. In Sec. IV our results are discussed and in the following, we verify our model by comparing the simulation results with the experimental results. Finally, the paper is concluded in Sec. V.

II. Device Description and Measurement Setup

A. SPAD Structure

Fig. 1 shows the cross section of the SPAD structure fabricated in a 0.35 μm OPTO-ASIC CMOS process which consists of a thick low-doped absorption region (p- epi) and a multiplication zone formed at the n^+/p-well junction. In this technology an anti-reflection coating layer is not available and the active area is coated by a thick inter metal level oxide and passivation stacks. When the device is exposed to light, photons will reach the silicon surface after passing through the isolation and passivation stacks. Due to the difference between refractive index of these different layers, a portion of the total photons is reflected at each interface. Therefore, it is expected that standing waves are formed in both isolation and passivation stack as a result of interference between transmitted and reflected waves traveling in opposite directions.

Furthermore, when the device is biased beyond the breakdown voltage (i. e. an excess bias is applied) the whole absorption region is depleted and a strong electric field is formed in the multiplication zone. This remarkably increases the thickness of the drift region where photons should be absorbed [17]. To avoid premature edge breakdown, the p-well is formed to be smaller than the n^+ region and also an n-well is formed at the edge of the n^+ region.

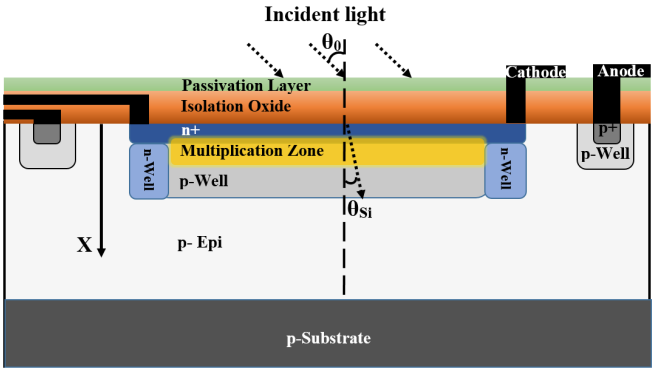

Fig. 1: Schematic cross section of the n^+/p-well CMOS SPAD (not to scale). Here, θ_0 denotes the angular deviation of the incident light from the surface normal and x indicates the depth inside the silicon.

B. PDP Measurement

The photon detection probability can be experimentally obtained as the ratio of the detected photons to the total number of impinging photons measured using a (calibrated) reference detector. One should note that an avalanche might be triggered without a photon being absorbed, but through the intrinsic SPAD parasitic mechanisms including the thermal generation of carriers (dark-count) or the release of trapped carriers (so-called after-pulsing). Therefore, the avalanche counts that are caused by the parasitics are excluded using the following equation:

$$\mathrm{PDP} = \frac{\left(\frac{\text{number of counts}}{1-\text{number of counts}.\mathrm{t_{dead}}} - \mathrm{n_{dark}}\right) \times (1 - \mathrm{p_{ap}})}{\text{Number of incident photons}}, \quad (1)$$

where $\mathrm{n_{dark}}$ is the dark-count rate and $\mathrm{p_{ap}}$ is the after-pulsing probability, which are obtained using the method presented in [18]. Eq. (1) includes the pile-up effect which is around 1% at the dead time (t_{dead}) of 9 ns. Here, to count the avalanche detection events, we used a National Instruments PXI system coupled with LabView in presence of the light flux of 5×10^6 photons/second on the SPAD with an active area diameter of 80 μm through a 62.5 μm multimode fiber coupled with a monochromator which swept the wavelength from 450 nm to 850 nm by steps of 1 nm. Because the diameter of the fiber (light source) is smaller than the diameter of the active area and it is placed by a distance of around 10 μm above the detector surface, the total light is illuminated within the active area and all incident photons have the chance to trigger an avalanche event. Accordingly, the PDP is calculated with respect to the total number of photons which means that the fill factor is equal to one. As a result, the PDP definition translates into the photon detection efficiency (PDE). It is worth mentioning that, in order to quench/reset the SPAD, a fast active quench/reset circuit with a dead time of 9 ns is used. Furthermore, the optical power is set well below the limit where any saturation or pile-up effect is observed. In other words, the average inter-arrival time is more than one order of magnitude longer than the detector dead-time.

III. PDP Modeling Approach

A. Background

As it was mentioned before, due to a non-zero reflection, not every incident photon is transmitted into the silicon. Furthermore, not every transmitted photon generates electron-hole pairs in an area where the carriers can initiate a self-sustaining avalanche event. In fact, the avalanche triggering probability (P_{av}), defined as the probability that a photo-generated electron-hole pair initiates an avalanche event, is a function of the absorption depth (x) (i. e. the electric field) and the diffusion length of carriers ($L_{\mathrm{e}}, L_{\mathrm{h}}$) as they may recombine before reaching the multiplication regions.

Accordingly, in a one-dimensional fashion along x (i. e. in the center of the device and across the area covered by the multiplication regions, where the electric field is vertical), the PDP is estimated as a function of two (independent) factors, the photon absorption probability (P_{ab}) and the avalanche triggering probability (P_{av}) given as

$$\mathrm{PDP}(\lambda, \theta_0, V_{\mathrm{ex}}) = \int_0^{x_{\mathrm{sub}}} P_{\mathrm{ab}}(\lambda, \theta_0, x) \times P_{\mathrm{av}}(V_{\mathrm{ex}}, x) dx, \quad (2)$$

where x_{sub} denotes the deepest point in the silicon substrate which is in the order of a few hundred micrometers (set to 350 μm in our simulation). Both P_{ab} and P_{av} strongly depend on x. Furthermore, as is explained later, $P_{\mathrm{ab}}(\lambda, \theta_0, x)$ is a function of the wavelength (λ) and the angular deviation of the incident light from the surface normal (θ_0) and $P_{\mathrm{av}}(V_{\mathrm{ex}}, x)$ is a function of the excess bias voltage (V_{ex}) which is defined as the difference between the applied reverse bias and the breakdown voltage.

Due to the structural symmetry (Fig. 1) and based on the fact that, the device diameter (80 μm) is around two orders of magnitude larger than the wavelengths of the light, both P_{ab} and P_{av} show strong dependencies on x but negligible variations in the other directions. Therefore, if we accurately obtain these two probabilities (as a function of x), the calculation of PDP reduces to a one-dimensional numerical integration problem which we have implemented in MATLAB.

Fig. 2 shows the flow chart of the presented methodology for modeling the PDP. It can be seen that $P_{\mathrm{av}}(V_{\mathrm{ex}}, x)$ and $P_{\mathrm{ab}}(\lambda, \theta_0, x)$ are extracted from TCAD and optical simulation, respectively to be used in Eq. 2. In TCAD simulation, the structure is defined based on the SPAD's layout and the PDK information as well as the doping profiles provided by the foundry. In order to simulate the device accurately and consider all physical effects, appropriate models for impact ionization, generation-recombination, and mobility have to be selected. In addition, a calibration of the impact ionization parameters is required to achieve a good fit to the measured data.

The optical simulation includes the definition of the light source, the boundary conditions, and the known optical and structural properties of the device (e.g. the silicon, oxide, and air refractive indexes) as well as a calibration of the optical properties of the isolation and passivation layers. Such calibration is necessary to achieve accurate optical simulation results, due to the lack of important technology information (e.g. the exact values of the isolation thickness or the refractive index of the passivation layers) that are not covered within the information provided by the foundry.

B. Optical Simulations

In order to obtain $P_{\mathrm{ab}}(\lambda, \theta_0, x)$, we propose to perform electromagnetic simulations as accurate calculation of the photon transmission and the absorption profile are essential. Accordingly, by considering the light as a wave, we can estimate its transmission properties at any wavelength to calculate the amount of light intensity inside the silicon. This amount divided by the total incident light intensity, is equivalent to the portion of the light entering the silicon and, when the light is considered as a photon, corresponds to the probability that a photon is transmitted into the silicon. Similarly, by taking the absorption coefficient of the silicon into account and obtaining the absorption profile of the light inside the silicon based on electromagnetic simulations, the photon absorption probability distribution can be obtained as a function of x.

Here, as the diameter of the active area is large enough compared to the wavelength, one can consider the light as a plane wave propagating along the x axis and having a uniform amplitude on any plane parallel to the active area (i.e. the silicon interface). This is a simplifying assumption to estimate $P_{\mathrm{ab}}(\lambda, \theta_0, x)$ as the photon absorption probability distribution multiplied by the probability that a photon is transmitted into the silicon at any λ and θ_0.

As it was explained before, the presented modeling approach includes a calibration of the optical properties of the isolation and passivation layers serving as degrees of freedom which, to a certain extent, can compensate the effect of any further assumption with respect to the exact light source properties and still provide a good agreement between model and experimental data. For example, it can be shown that if the effect of a non-zero beam angle of the light source is taken into account in the optical simulation, a good agreement between model and experimental data is still achievable by adjusting the properties of the isolation and passivation layers.

Furthermore, we should highlight that, due to the high sensitivity of the SPAD device (at single photon level) and in order to avoid the detector saturation due to the pile-up effect, the SPAD is usually exposed to a very low optical power in its functional application mode. Therefore, at such a low optical power with countable photons, the interference between several waves or wave packets is less significant as compared to that of a single (monochromatic) wave with itself. Accordingly, the assumption of a monochromatic wavelength to estimate the transmission probabilities of a single photon seems justified.

C. TCAD Simulations

In the case that a photon is absorbed in the depletion region, the generated electron and hole are promptly separated

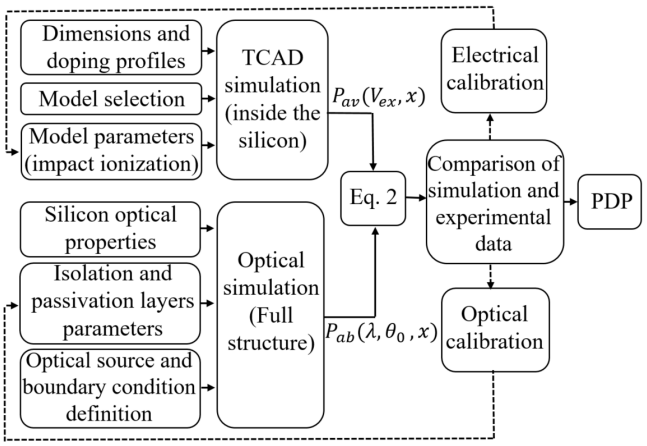

Fig. 2: Flow chart of the PDP modeling procedure.

(drifting in opposite directions) by the electric field and the minority carrier is accelerated towards the multiplication region. When the photon is absorbed in a neutral region, the generated carriers may result in an avalanche only if they diffuse into the depletion region. As not every carrier can diffuse into the depletion zone, one should take the recombination probability into account to obtain the total avalanche triggering probability. Consequently, depending on the absorption depth (x), an avalanche may be triggered either by a generated electron or a hole. The total avalanche triggering probability, therefore, can be obtained in accordance with the probabilities that an electron or a hole may trigger an avalanche event as two independent events. As a result, $P_{\rm av}$ corresponds to the probability of an inclusive event and is given by

$$P_{\rm av}(V_{\rm ex},x) = [P_{\rm e}(V_{\rm ex},x) + P_{\rm h}(V_{\rm ex},x) - P_{\rm e}(V_{\rm ex},x)\times P_{\rm h}(V_{\rm ex},x)] \times P_{\rm diff}(x). \quad (3)$$

Here, $P_{\rm diff}(x)$ is the probability that a photo-generated minority carrier diffuses into the depletion region through the neutral region. This term is equal to 1 when x is in the depletion region and $P_{\rm diff}(x)$ is obtained by the following equation when x is in the neutral regions. It is worth mentioning that, unlike the common appellation that defines the avlanche probability only in the multiplication region and consider it as null elsewhere, here the total avalanche probability ($P_{\rm av}$) represents an effective value that takes the avalanche probabilities of the diffused and drifted carriers which are generated outside the multiplication region into account.

$$P_{\rm diff}(x) = \begin{cases} e^{-(\frac{w_1-x}{L_{\rm h}})} & \text{neutral n-type (above),} \\ e^{-(\frac{x-w_2}{L_{\rm e}})} & \text{neutral p-type (below),} \end{cases} \quad (4)$$

where $L_{\rm h}$ ($L_{\rm e}$) represents the diffusion length of the holes (electrons) and w_1 (w_2) corresponds to the top (bottom) boundary of the neutral regions to the depletion zone.

Now, under a certain excess bias voltage, $P_{\rm e}(V_{\rm ex},x)$ and $P_{\rm h}(V_{\rm ex},x)$ are obtained by solving a set of two coupled equations [19] given by

$$\begin{aligned} \frac{\partial P_{\rm e}}{\partial x} &= (1-P_{\rm e})\gamma_{\rm e}(P_{\rm e}+P_{\rm h}-P_{\rm e}P_{\rm h}), \\ \frac{\partial P_{\rm h}}{\partial x} &= (1-P_{\rm h})\gamma_{\rm h}(P_{\rm e}+P_{\rm h}-P_{\rm e}P_{\rm h}). \end{aligned} \quad (5)$$

Here, $\gamma_{\rm e}$ and $\gamma_{\rm h}$ denote the electron and hole impact ionization coefficients, respectively.

These two parameters justify the strong dependency of the avalanche probabilities on the excess bias and are obtained by performing TCAD simulations as is explained in the next section. In the following, we discuss how the above-mentioned modeling and simulation considerations are applied and compare the obtained results with the experimental data.

IV. Results and Discussion

A. Optical Considerations

Fig. 3 shows the measured PDP spectrum (dotted curve) using the SPAD structure and the approach explained in Sec.II. The wavelength-dependent fluctuations of the PDP are due to the formation of standing waves in the isolation and the passivation layers above the silicon which, to the best of our knowledge, has been ignored in the previously presented PDP modeling efforts [11]–[14]. We believe that this effect needs a careful consideration as it is expected to arise in SPAD devices implemented in standard CMOS technologies, where an anti-reflection coating is usually not available.

By a closer look into the measured spectrum, we observe an envelope over the main (faster) fluctuations with λ. Intuitively, this can be considered as the presence of two standing waves formed in the isolation (i. e. intermediate) and the passivation layers, where the faster fluctuation corresponds to the standing wave in the (thicker) isolation layer and the envelope corresponds to the standing wave in the passivation layer with an optical thickness of around one-tenth of the isolation layer. In fact, as in a thicker layer a larger number of nodes and antinodes (i. e. $\lambda/2$ fractions) of a standing wave are formed, a change in λ accumulates over all these fractions and, therefore, it shows a higher fluctuation rate in the spectrum. As a result, when the thickness of a layer is much smaller, its corresponding fluctuation is observed as an envelope of the faster fluctuations.

To better understand this effect and provide more accurate PDP modeling results, electromagnetic simulation was performed using the CST Microwave Studio simulation tool [20]. The obtained results regarding the optical transmission as a function of λ and based on the SPAD structure (Fig. 1) and accurate PDK information provided by the foundry is shown in Fig. 3. This result proves that the fluctuations in the PDP spectrum are due to the λ-dependent reflection/transmission of the photons and accurate calculation of the photon absorption probability is possible only when this effect is accounted for.

Indeed, as it was explained before, when the photon-transmission and the photon absorption profile inside the silicon are accurately represented, $P_{\rm ab}$ can be obtained by multiplying these values. The photon absorption profile is usually simply estimated by $\alpha \cdot exp(-\alpha x)$, where α denotes the absorption coefficient and is a function of λ. A more accurate calculation of photon absorption profile can be determined as the normalized light intensity obtained by electromagnetic

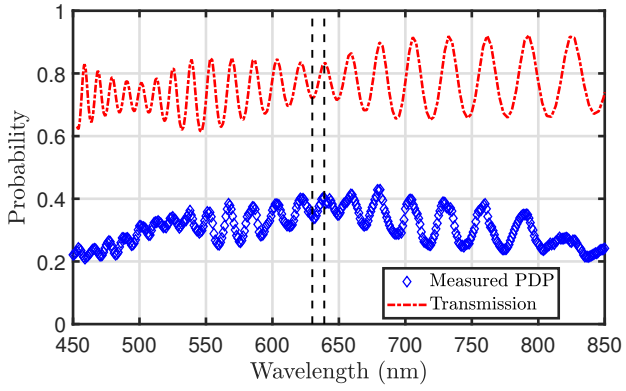

Fig. 3: The optical transmission into the silicon (simulated at $\theta_0 = 0$) and the measured PDP spectrum (at $\theta_0 = 0$ and $V_{\rm ex} = 6.6\ V$).

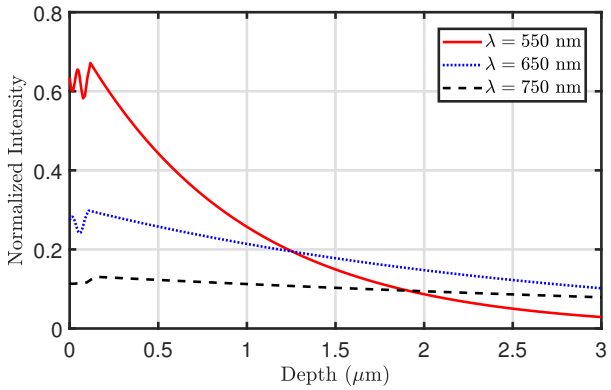

Fig. 4: Normalized light intensity as a function of depth x for three different values of λ at $\theta_0 = 0$.

simulations as is shown in Fig. 4.

It is interesting to note that the profile does not exactly follow an exponential decay which is the expected behavior for the absorption profile inside the silicon [12]–[14]. We believe that the interference observed below the surface of the silicon (close to ($x = 0$) is due to the penetration of the standing wave formed in the isolation layer into the silicon. In fact, the absorption profile inside the silicon is different from an exponential decay starting at the surface (x=0), as the boundary condition at the silicon surface is different from an interface of two materials extended to infinity from the other side. Therefore, the interference between waves reflected back and forth in the isolation layer penetrates into the silicon and affects the absorption profile inside the silicon where the exponential decay is shifted away from the silicon surface by ∼200 nm.

In order to calculate the PDP accurately, one should take this interference effect into account especially as in the CMOS-implemented SPADs the multiplication zone is very shallow and close to the surface. Additionally, at shorter wavelengths a significant portion of arriving photons are absorbed close to the surface inside the silicon. For instance, at λ from ∼400 nm to 500 nm around half of the transmitted photons are absorbed within the depth range x =0 to 200 nm.

TABLE I: Summary of the parameters used in the TCAD simulation performed by ATLAS and the extracted boundaries of the depleted zone to be use in Eq. 3 at an excess bias voltage of 6.6 V.

Parameter	Discription	Value
an	Impact ionization constant	7.03×10^5 1/cm
En_crit	for electron [21]	1.231×10^6 V/cm
ap	Impact ionization constants	1.58×10^6 1/cm
Ep_crit	for hole [21]	2.036×10^6 V/cm
V_br	Breakdown voltage	25 V
taun	Electron life time	200 μs
taup	Hole life time	200 μs
L_e	Electron diffusion length	270 μm
L_h	Hole diffusion length	90 μm
W1	Top boundary of depleted region	220 nm
W2	Bottom boundary of depleted region	12.5 μm

B. Electrical Considerations

In order to obtain the avalanche triggering probability required in Eq. 1, we need to perform TCAD simulations. More specifically, the impact ionization coefficients (Eq. 5) as a function of x and the two-dimensional electric field (to obtain $E(x)$ for all possible incidence angles) has to be calculated using TCAD simulations to estimate the electron and hole avalanche triggering probabilities to be used in Eq. 2. The key parameters and the corresponding values that are used in the simulations are shown in Table I.

Fig. 5a shows a two-dimensional plot of the electric field at an excess bias voltage of 6.6 V simulated using the Geiger-mode device simulation feature of SILVACO Atlas [22]. The boundaries of depleted region are obtained and indicated to distinguish the neutral regions and the depletion zone. The dimensions of the depleted region strongly depend on the applied reverse bias and this effect is much more observable at voltages below the breakdown where the device is not fully

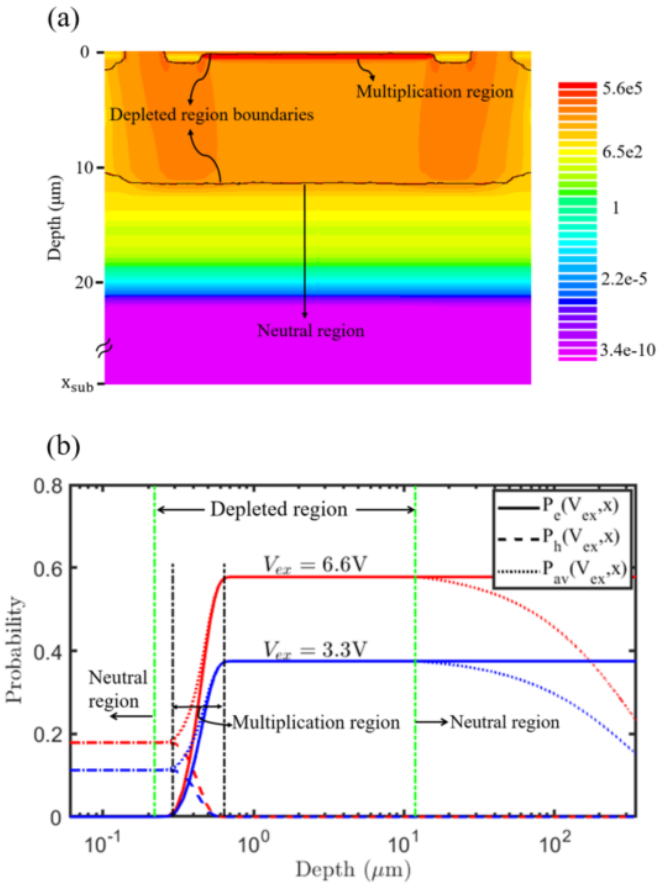

Fig. 5: (a) Simulated 2D electric field and the depletion region boundaries of the n$^+$/p-well CMOS SPAD at V_{ex}= 6.6 V in logarithmic scale. (b) Electron and hole avalanche triggering probability distributions for excess biases of 3.3 V and 6.6 V at $\theta_0 = 0$.

depleted (down to the substrate). However, for reverse biases higher than a specific level, the device enters full depletion, which means that the increase of the reverse bias will have a small effect on w_1 and w_2 in the range of nanometer.

Fig. 5b shows the electron, hole, and effective (total) avalanche triggering probability distributions as a function of x for different excess bias voltages. Although the avalanche process happens only in the multiplication region, a carrier generated outside this region can reach the multiplication region and result in an avalanche event. Therefore, below the multiplication zone and inside the depletion region, $P_{\rm av}(x)$ is equal to $P_{\rm e}(x)$ and shows a constant value. This is due to the fact that an electron generated at any x in this region, will pass across the whole multiplication region to reach the cathode through $\rm n^+$. In addition, the effect of recombination in this region is negligible due to a strong drift of the carriers with opposite directions for electrons and holes. On the other hand, when the electron is generated above the multiplication region, it is transferred towards the cathode without flowing through the multiplication region and, thus, $P_{\rm e}$ is equal to zero close to the silicon surface.

It is clear that for electrons generated inside the multiplication region, $P_{\rm e}$ increases with x from zero to a maximum value. A similar argument applies to the holes but in a reverse manner with x, as the holes are transferred towards the anode. Due to a smaller impact ionization coefficient associated with the holes compared to that of the electrons, the maximum value of $P_{\rm h}$ is smaller than the maximum $P_{\rm e}$. It is expected that by increasing the excess bias, a stronger electric field is applied across the multiplication region and therefore, both electron and hole impact ionization rates ($\gamma_{\rm e}$ and $\gamma_{\rm h}$) are increased. As a result, both avalanche triggering probabilities ($P_{\rm e}$ and $P_{\rm h}$) are increased for V_{ex}=6.6 V as shown in Fig. 5b.

It is important to note that the neutral regions outside the depleted region (equivalent to the region x $<$ 0.2 μm and the region 12.5 μm $<$ x $<$ $x_{\rm sub}$), a photo-generated minority carrier diffuses into the depletion region with a probability calculated by Eq. 4, and then is accelerated towards the multiplication zone to trigger an avalanche event. Therefore, a photon absorbed in a neutral region has a chance to make a contribution to the effective avalanche probability $P_{\rm av}$ as is shown in Fig. 5b.

By now, we have a rather clear understanding of how likely the generated carriers will trigger avalanche events in different regions inside the silicon at different biasing levels. To provide further insight, Fig. 6 shows the normilized photon absorption probabilities corresponding to different regions as a function of wavelength. It demonstrates that only at shorter wavelengths (λ $<$ 500 nm) a considerable portion of the transmitted photons are absorbed in the neutral region above the depletion region, while over the rest of the spectrum, photons are majorly absorbed in the depletion region. One should note that here the values are normalized to the total absorption at each wavelength and thus, the sum of relative absorptions is equal to 100 % at each wavelength. In fact, this figure only compares the contributions of different regions to the total absorption for each specific wavelength to emphasize the relative absorptions in the neutral regions for shorter and longer wavelengths.

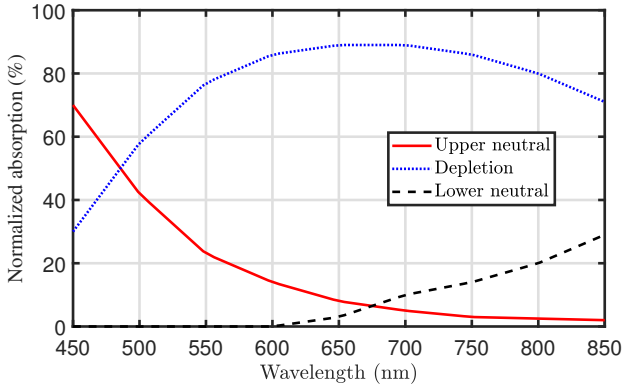

Fig. 6: Normalized contribution of upper neutral, depletion, and lower neutral regions to the photon absorption probabilities as a function of wavelength ($\theta_0 = 0$).

A quick observation of Fig. 5b and Fig. 6 reveals that at shorter wavelengths the PDP of our SPAD structure is mainly determined by holes generated close to the surface and, therefore, a lower PDP is expected as compared to higher wavelengths as the maximum avalanche triggering probability of electrons is about three times more than that of the holes. In the following, we present the PDP measurement and modeling results where the validity of the presented modeling approach can be inspected.

C. Verification of the Results

In order to verify our simulation and modeling results from the optical point of view, we calculate the PDP as a function of wavelength and compare the result with our measurement data. In fact, for a specific λ, it is possible that, for different assumptions over the thickness of the intermediate layers as well as the effective refractive index of the silicon nitride based passivation layer, the calculated optical transmission results in a good fit between the simulation and the experimental data. However, when we sweep λ, the modeling and simulation result can fit the experimental data only when the estimation approach is efficient and these assumptions are physically reasonable.

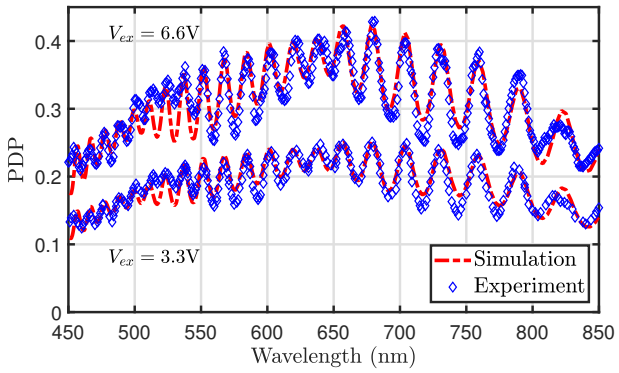

Fig. 7: Measured and simulated photon detection probability as a function of λ ($\theta_0 = 0$).

Fig. 7 depicts this verification approach by comparing the calculated and the measured spectrum for two different values of the excess bias. This demonstrates the effectiveness of the applied approach and these assumptions over the parameters of the intermediate layers in the CMOS technology. Unfortunately, we are not allowed to provide more technology details that are considered as confidential. It is worth mentioning that the PDP spectra at different excess bias voltages show the same dependency on the wavelength as varying the applied voltage only affects the avalanche probability but not the optical absorption (i. e. the photon transmission) probability.

From the electrical point of view, one can inspect the validity of the modeling approach by sweeping the applied excess bias voltage on the SPAD device. In fact, at a given biasing, it is possible that different assumptions over the doping profiles and the parameters used for TCAD simulation (Table I), the calculated avalanche triggering probability and accordingly, the estimated PDP show a good fit to the experimental results. Nevertheless, if the biasing is varied, a good match between the modeling and the experimental data can be achieved when the applied approach and the underlying assumptions over the device characteristics happen to be valid.

Fig. 8a compares the obtained PDP based on the previously discussed modeling and measurement approaches as a function of the excess bias voltage for different wavelengths. It is clear that due to the increase of the avalanche triggering probabilities with the excess bias, the PDP is increased for higher voltages. The obtained result proves that, above a specific threshold (∼2 V), the PDP shows a linear increase with the excess bias. This is consistent with the fact that the strength of the electric field in the multiplication zone shows a linear increment with the voltage level. Furthermore, according to our simulation results for the studied structure, the thickness of the depleted region shows a negligible variation with the voltage changes above breakdown. Otherwise, the PDP may exhibit an increase rate faster than linear.

At a first glance, Fig. 8a shows different increase rates corresponding to different wavelengths. However, if we plot the normalized PDP values as is shown in Fig. 8b, it becomes clear that the behavior of the PDP as a function of the excess bias is independent of the wavelength. It is worth mentioning that, at each wavelength, the PDP is normalized to its value at an excess bias of 7 volt.

It is important to note that below a specific excess bias voltage (here ∼2 V), the experimental measurement of the PDP is significantly affected by the readout sensitivity of the electronic circuit which is not considered in the presented modeling and simulation approach. In fact, we believe that due to the random nature of the avalanche process and depending on the readout sensitivity, there is a specific excess bias level below which, some of the detection (i. e. avalanche) events are not counted (distinguished) by the readout circuitry as (randomly) the amount of the avalanche-generated charge falls below a specific amount. However, when the excess bias is higher than this specific value, there is a negligible change to have such weak avalanche events which cannot be distinguished and, therefore, the experimental measurement of the PDP is not affected by the readout sensitivity of electronics.

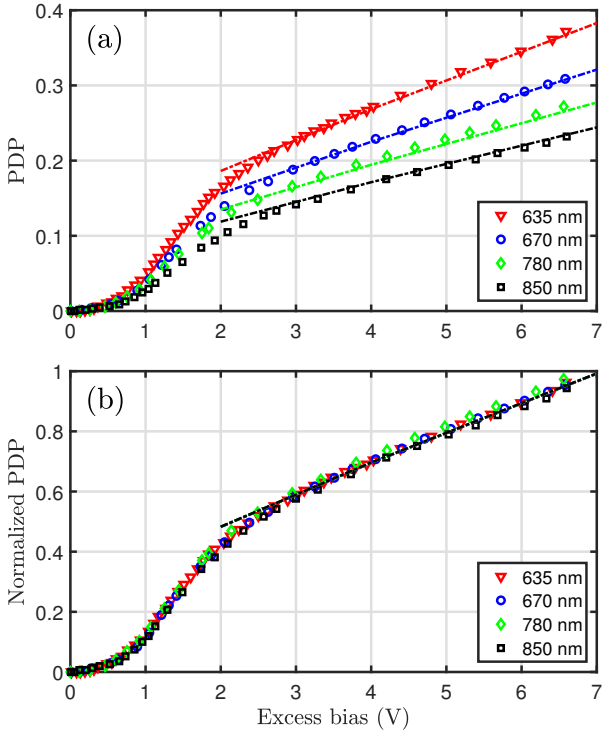

Fig. 8: The obtained (a) and normalized (b) PDP based on experiment and simulation (dashed lines) data as a function of excess bias at different wavelengths ($\theta_0 = 0$).

D. Further Discussions

In order to highlight the advantages of the presented modeling and simulation approach, Fig. 9a shows the dependency of the PDP to the angular deviation of the incident light (θ_0) for two different wavelengths which correspond to a local PDP maximum (637 nm) and minimum (630 nm) in the PDP spectrum (Fig. 3). In general, the avalanche probability is independent of θ_0. However, the absorption probability changes with θ_0 mainly as the photon transmission (reflection) is a function of θ_0 as is shown in Fig. 9a. Furthermore, due to the fact that a non-zero θ_0 results in a non-zero deviation from the surface normal inside the silicon (shown as θ_{Si} in Fig. 9b), the absorption profile in the silicon (e.g. Fig. 4) is affected as, at a given x, the light takes a longer trajectory (by a factor of $1/\cos(\theta_{\mathrm{Si}})$) for an increased θ_{Si}. Therefore, we expect that the average absorption depth is decreased when θ_{Si} is increased. However, according to our simulation results, this has a negligible effect on the PDP as θ_{Si} is much smaller than θ_0 due to the high refractive index of the silicon. For example, even for $\theta_0 = 60°$ the light trajectory (i.e. the absorption depth) is scaled by a factor of 1.03.

According to Fig. 9, the PDP deceases with increasing θ_0 as the reflection will increase and less photons reach the silicon. Nevertheless, the PDP curves exhibit θ_0-dependent fluctuations where the two curves show a reverse behavior increasing θ_0 from zero. In fact, at the beginning ($0 < \theta_0 < 10°$), the

curve corresponding to the maximum (minimum) decreases (increases) with θ_0.

Intuitively, from the optical point of view, the increase of θ_0 at a fixed λ (Fig. 9a) is equivalent to the decrease of λ at $\theta_0 = 0$ (Fig. 3) as at a higher deviation of the incidence angle from the surface normal the light sees a longer trajectory inside the intermediate layers. More clearly, the increase of the length of the trajectory has a similar effect as the decrease of λ on the formation of a standing wave. Therefore, the PDP behavior shown in Fig. 9a can be understood by referring to the PDP spectrum (Fig. 3), where by decreasing λ (going to the left), the PDP decreases with λ if the starting point is λ =637 nm while it increases if the observation start from λ =630 nm.

The θ_0-dependent characterization of the PDP is mostly motivated by practical detector design and applications, where the maximum detection angle corresponding to a minimum acceptable PDP is a critical parameter (e. g. optical wireless communication [23]). However, this can be very difficult or time consuming to conduct experimentally and, therefore, the application of a verified and reliable modeling and simulation approach as is presented here can be very helpful to provide insight into the detector performance. In the end, we believe that the presented flow (as shown in Fig. 2) covers a comprehensive PDP modeling procedure as it includes both optical and TCAD aspects and may be extended to other SPAD structures by adopting the TCAD and/or the optical simulation accordingly. For example, a similar procedure can be followed to study the PDP characteristics of backside illuminated (BSI) SPADs where optical simulation is adopted to accurately capture the photon absorption probability. However, for SPAD technologies with small pixel pitches (e.g. large SPAD array), where the fill factor plays an important role in the photon detection properties of the device, an extension of the numerical integration in accordance with Eq. 2 to a two-dimensional integral seems necessary. Such extension could be a challenging and interesting topic for further research.

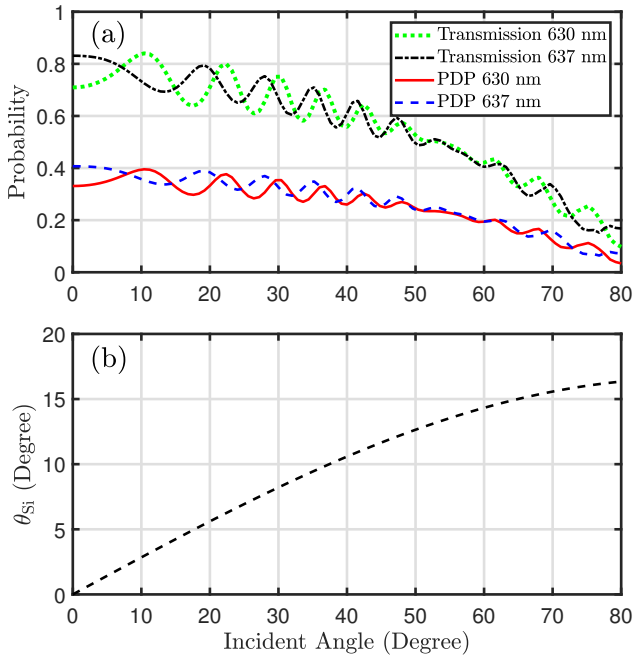

Fig. 9: (a) The optical transmission and the PDP as a function of θ_0 at $V_{ex} = 6.6$ V. (b) Angular deviation of the light in the silicon from the surface normal (θ_{Si}) according to θ_0.

V. Conclusion

A comprehensive model is presented to characterize the PDP performance of a CMOS-implemented SPAD structure. It is shown that due to the presence of a standing wave effect and the complex dependency of the PDP on different optical and electrical parameters, an accurate modeling and simulation approach is necessary. This is more critical when an anti-reflection coating is not available and can be the case in many CMOS technologies. The validity of the presented approach is demonstrated by achieving an excellent consistency between the simulation and experimental measurement results. The presented approach can be used for accurate PDP characterization and proves useful to considerably reduce the effort required for experimental-based characterization and optimization in different CMOS SPAD applications.

Acknowledgment

The authors acknowledge financial support from the Austrian Science Fund (FWF, grant no. P28335-N30).

References

[1] S. Afshar, T. J. Hamilton, L. Davis, A. Van Schaik, and D. Delic, "Event-based Processing of Single Photon Avalanche Diode Sensors," *IEEE Sensors Journal*, vol. 20, no. 14, pp. 7677–7691, 2020.

[2] D. Thomas, J. Michailos, and K. Rochereau, "Challenges and Capabilities of 3D Integration in CMOS Imaging Sensors," in *49th European Solid-State Device Research Conference (ESSDERC)*. IEEE, 2019, pp. 54–56.

[3] E. Fisher, I. Underwood, and R. Henderson, "A Reconfigurable Single-Photon-Counting Integrating Receiver for Optical Communications," *IEEE J. Solid-State Circuits*, vol. 48, no. 7, pp. 1638–1650, 2013.

[4] H. Zimmermann, B. Steindl, M. Hofbauer, and R. Enne, "Integrated Fiber Optical Receiver Reducing the Gap to the Quantum Limit," *Sci. Rep.*, vol. 7, no. 1, p. 2652, 2017.

[5] R. K. Henderson, N. Johnston, F. M. Della Rocca, H. Chen, D. D.-U. Li, G. Hungerford, R. Hirsch, D. McLoskey, P. Yip, and D. J. Birch, "A 192 × 128 Time Correlated SPAD Image Sensor in 40-nm CMOS Technology," *IEEE J. Solid-State Circuits*, vol. 54, no. 7, pp. 1907–1916, 2019.

[6] C. Bruschini, H. Homulle, I. M. Antolovic, S. Burri, and E. Charbon, "Single-Photon Avalanche Diode Imagers in Biophotonics: Review and Outlook," *Light: Science & Applications*, vol. 8, no. 1, pp. 1–28, 2019.

[7] V. Savuskan, M. Javitt, G. Visokolov, I. Brouk, and Y. Nemirovsky, "Selecting Single Photon Avalanche Diode (SPAD) Passive-Quenching Resistance: An Approach," *IEEE Sensors Journal*, vol. 13, no. 6, pp. 2322–2328, 2013.

[8] R. Enne, B. Steindl, M. Hofbauer, and H. Zimmermann, "Fast Cascoded Quenching Circuit for Decreasing Afterpulsing Effects in 0.35-μm CMOS," *IEEE Solid-State Circuits Letters*, vol. 1, no. 3, pp. 62–65, 2018.

[9] F. Zappa, A. Lotito, A. Giudice, S. Cova, and M. Ghioni, "Monolithic Active-Quenching and Active-Reset Circuit for Single-Photon Avalanche Detectors," *IEEE Journal of Solid-State Circuits*, vol. 38, no. 7, pp. 1298–1301, 2003.

[10] V. Savuskan, I. Brouk, M. Javitt, and Y. Nemirovsky, "An Estimation of Single Photon Avalanche Diode (SPAD) Photon Detection Efficiency (PDE) Nonuniformity," *IEEE Sensors Journal*, vol. 13, no. 5, pp. 1637–1640, 2013.

[11] M. Mazzillo, A. Piazza, G. Condorelli, D. Sanfilippo, G. Fallica, S. Billotta, M. Belluso, G. Bonanno, L. Cosentino, A. Pappalardo *et al.*, "Quantum Detection Efficiency in Geiger Mode Avalanche Photodiodes," *IEEE Trans. Nucl. Sci.*, vol. 55, no. 6, pp. 3620–3625, 2008.
[12] Y. Xu, P. Xiang, X. Xie, and Y. Huang, "A New Modeling and Simulation Method for Important Statistical Performance Prediction of Single Photon Avalanche Diode Detectors," *Semiconductor Science and Technology*, vol. 31, no. 6, p. 065024, 2016.
[13] G. Gallina, F. Retière, P. Giampa, J. Kroeger, P. Margetak, S. B. Mamahit, A. D. S. Croix, F. Edaltafar, L. Martin, N. Massacret *et al.*, "Characterization of SiPM Avalanche Triggering Probabilities," *IEEE Trans. Electron Devices*, vol. 66, no. 10, pp. 4228–4234, 2019.
[14] C.-A. Hsieh, C.-M. Tsai, B.-Y. Tsui, B.-J. Hsiao, and S.-D. Lin, "Photon-Detection-Probability Simulation Method for CMOS Single-Photon Avalanche Diodes," *Sensors*, vol. 20, no. 2, p. 436, 2020.
[15] T. Leitner, A. Feiningstein, R. Turchetta, R. Coath, S. Chick, G. Visokolov, V. Savuskan, M. Javitt, L. Gal, I. Brouk *et al.*, "Measurements and simulations of low dark count rate single photon avalanche diode device in a low voltage 180-nm cmos image sensor technology," *IEEE Transactions on Electron Devices*, vol. 60, no. 6, pp. 1982–1988, 2013.
[16] S. S. Kohneh Poushi, H. Mahmoudi, B. Steindl, M. Hofbauer, and H. Zimmermann, "Comprehensive Modeling of Photon Detection Probability in CMOS-Based SPADs," in *2020 IEEE Sensors*, 2020, "in print".
[17] B. Steindl, R. Enne, and H. Zimmermann, "Thick Detection Zone Single-Photon Avalanche Diode Fabricated in 0.35 μm Complementary Metal-Oxide Semiconductors," *Optical Engineering*, vol. 54, no. 5, p. 050503, 2015.
[18] H. Mahmoudi, M. Hofbauer, B. Steindl, K. Schneider-Hornstein, and H. Zimmermann, "Statistical Study of Intrinsic Parasitics in an SPAD-Based Integrated Fiber Optical Receiver," *IEEE Transactions on Electron Devices*, vol. 66, no. 1, pp. 497–504, 2018.
[19] R. J. McIntyre, "On the Avalanche Initiation Probability of Avalanche Diodes Above the Breakdown Voltage," *IEEE Trans. Electron Devices*, vol. 20, no. 7, pp. 637–641, 1973.
[20] CST User's Manual. CST Microwave Studio. [Online]. Available: https://www.3ds.com
[21] R. Van Overstraeten and H. De Man, "Measurement of the Ionization Rates in Diffused Silicon pn Junctions," *Solid-State Electronics*, vol. 13, no. 5, pp. 583–608, 1970.
[22] Silvaco International. Atlas Manual. [Online]. Available: https://www.silvaco.com
[23] D. Milovančev, T. Jukić, B. Steindl, P. Brandl, and H. Zimmermann, "Optical Wireless Communication Using a Fully Integrated 400 μm Diameter APD Receiver," *The Journal of Engineering*, vol. 2017, no. 8, pp. 506–511, 2017.

Hiwa Mahmoudi received the M.Sc. and Ph.D. degrees from the Sharif University of Technology, Tehran, Iran, and Vienna University of Technology, Vienna, Austria, in 2009 and 2014, respectively.

Since 2014, he has been with the Institute of Electrodynamics Microwave and Circuit Engineering, Vienna University of Technology, as a Post-Doctoral Researcher, focusing on simulation and analysis of integrated circuits.

Saman Kohneh Poushi received the M.Sc degree in electrical engineering from the Tarbiat Modares University, Tehran, Iran, in 2013.

In 2014, he joined the academic center for education, culture and research, Tehran, Iran, working on quantum dot based solar cells. Since 2019 he has been with the Institute of Electrodynamics Microwave and Circuit Engineering, Vienna University of Technology, pursuing his Ph.D. degree on simulation and characterization of CMOS APD/SPAD detectors.

Bernhard Steindl received the Dipl.-Ing. degree and the Dr. techn. degree from Vienna University of Technology, Vienna, Austria, in 2013 and 2019, respectively. In 2011, he joined the Institute of Electrodynamics, Microwave and Circuit Engineering, Vienna University of Technology, doing his master thesis on characterization of APDs. He has authored and co-authored over 20 journal and conference papers. His research interests include optoelectronics, APDs, SPADs, and simulation of semiconductor devices.

Michael Hofbauer received the Dipl.-Ing. degree in electrical engineering, and the Ph.D. degree (Hons.) Sub auspiciis Praesidentis from the Vienna University of Technology (TU Wien), Vienna, Austria, in 2011 and 2017, respectively. Since 2005, he has been as student worker and project assistant with the Institute of Electrodynamics Microwave and Circuit Engineering, TU Wien, where he became an University Assistant in 2016. His interests are in electronic-photonic integration and optical metrology. He has authored and coauthored over 60 publications.

Horst Zimmermann (SM'02) received the Dr.-Ing. degree from Univ. Erlangen-Nürnberg, Germany, in 1991. Then he was an Alexander-von-Humboldt Research-Fellow at Duke University, Durham, N. C., working on diffusion in Si, GaAs, and InP. In 1993, he joined Kiel University, Germany, working on optoelectronic integration and finishing habilitation in 1999. Since 2000, he has been full professor for circuit engineering with Vienna University of Technology, working on (Bi)CMOS analog and optoelectronic full-custom design. He is author and coauthor of more than 550 publications and seven Springer books. In 2002, he became Senior Member IEEE.